Remote Sensing of Environment 186 (2016) 416–427

Contents lists available at ScienceDirect

Remote Sensing of Environment

journal homepage: www.elsevier.com/locate/rse

A study of the time evolution of GERB shortwave calibration by comparison with CERES Edition-3A data

R. Parfitt [a,*], J.E. Russell [a], R. Bantges [a,b], N. Clerbaux [c], H. Brindley [a,b]

[a] Department of Physics, Imperial College London, UK
[b] NERC National Centre for Earth Observation, UK
[c] Royal Meteorological Institute of Belgium, Belgium

ARTICLE INFO

Article history:
Received 14 January 2016
Received in revised form 8 August 2016
Accepted 7 September 2016
Available online xxxx

Keywords:
Earth Radiation Budget
GERB
CERES
Instrument calibration

ABSTRACT

This study examines the evolution of the GERB-2 and GERB-1 Edition 1 shortwave radiance calibration between 2004–2007 and 2007–2012 respectively, through comparison with CERES instrument FM1 Edition 3A SSF instantaneous radiances. Two periods when simultaneous observations from both GERB-2 and GERB-1 were available, January 13th to February 11th 2007 and May 1st to May 10th 2007, are also compared. For these two overlap periods respectively, averaged over all CERES 'unfiltered-to-filtered radiance ratio' subsets, the GERB-1/CERES unfiltered radiance ratio is on average found to be 1.6% and 1.9% lower than the associated GERB-2/CERES unfiltered radiance ratio. Over the two longer time series the GERB/CERES unfiltered radiance ratio shows a general decrease with time for both GERB-2 and GERB-1. The rate of decrease varies through time but no significant seasonal dependence is seen. Averaged over all subsets the GERB-2/CERES unfiltered radiance ratio showed a decrease of 1.9% between June 2004 and June 2006. Between June 2007 and June 2012, the corresponding decrease in the GERB-1/CERES unfiltered radiance ratio was 6.5%. The evolution of the GERB/CERES unfiltered radiance ratio for both GERB-2 and GERB-1 shows a strong dependence on the CERES unfiltered-to-filtered radiance ratio, indicating that it is spectrally dependent. Further time-series analysis and theoretical work using simulated spectral radiance curves suggests that for GERB-1 the evolution is consistent with a darkening in the GERB shortwave spectral response function which is most pronounced at the shortest wavelengths. For GERB-2, no single spectral cause can be identified, suggesting that the evolution is likely due to a combination of several different effects.

1. Introduction

The Geostationary Earth Radiation Budget (GERB, Harries et al., 2005) instruments are a series of broadband radiometers operating from geostationary orbit aboard the Meteosat Second Generation (Schmetz et al., 2002) satellites. The first GERB instrument (GERB-2) was operational aboard Meteosat-8 from March 2004 to May 2007, after which time the second GERB instrument (GERB-1) on Meteosat-9 provided measurements which extended to January 2013. One goal of the GERB mission is to provide a stable climate quality long-term dataset, with high absolute radiometric accuracy. As such, identifying and correcting for drifts in the instrument calibration that occur in orbit is a fundamental requirement. For the GERB Edition 1 data which are used in this study, the calibration of the individual GERB instruments are maintained independently using their on-board calibration sources. Fixed pre-launch measurements of their respective spectral responses are used in the processing.

Nevertheless, the wide field of view of the GERB instruments, as well as their mounting on the spinning Meteosat platform means that they will inevitably be exposed to significant amounts of ultraviolet (UV) radiation during normal operation. Despite the presence of on-board calibration targets, the effect on calibration of long-term exposure of any optical system to UV radiation has long been an outstanding problem for Earth Observation sensors (e.g. Clark and DiBattista, 1978). As such, there is some expectation that a change in the detail of the GERB spectral response during operation will occur. Additionally, preliminary studies of the GERB Edition 1 data have shown apparent scene-dependent decreases in the derived shortwave (SW) fluxes over the course of the instrument lifetimes (Russell, 2011, N. Clerbaux, personal comm., April 2015). For these reasons, the present study has been undertaken as part of a larger effort to survey the GERB Edition 1 data record for artefacts and spurious trends due to instrument and processing effects that can only be discerned after some years of data are available.

In this study, unfiltered SW radiances from the GERB-2 and GERB-1 instruments are compared to analogous observations from the Clouds and the Earth's Radiant Energy System (CERES, Wielicki et al., 1996), on the polar orbiting Terra satellite. The CERES broadband instruments are particularly suited as their optics and processing offer many

* Corresponding author at: Space and Atmospheric Physics Department, Imperial College London, London SW7 2AZ, UK.
E-mail address: r.parfitt10@imperial.ac.uk (R. Parfitt).

http://dx.doi.org/10.1016/j.rse.2016.09.005

similarities to the GERB instruments, such as Denton enhanced silver-coated mirrors, the use of a quartz filter in the SW region and the use of a scene dependent spectral correction to derive unfiltered radiances (Loeb et al., 2001). The calibration and stability of the CERES instruments have also been extensively studied through inter-comparison between the different flight models and with other instruments to ensure their long-term climate accuracy (Loeb et al., 2006; Priestley et al., 2011; Shankar et al., 2014). Moreover, a previous analysis of the CERES instruments (Matthews et al., 2005) identified a spectral darkening of their SW optics, resulting from a process similar to that suspected in the GERB instruments.

Given the relatively similar start of life calibration uncertainties of the two datasets, 1% for CERES (Wielicki et al., 1996) and 2.25% for GERB (Russell, 2011), this study concentrates on the evolution of the calibration differences between GERB and CERES rather than the initial bias between the datasets. Changes are interpreted here in terms of a calibration drift in the GERB radiances. This is considered as a reasonable first approximation given the independent evidence of a possible trend in the GERB SW fluxes, the work already carried out to ensure and validate the stability of the Edition 3A CERES data, and the operational constraints placed on the CERES Flight Model 1 (FM1) instrument throughout the period considered to minimise its UV exposure. Additionally, as a first step to understanding the underlying mechanism behind the identified changes, we perform a short theoretical study, using simulated spectral radiance curves for a variety of different scenes from the NASA Advanced Spaceborne Thermal Emission and Reflection Radiometer (ASTER) spectral library (Baldridge et al., 2009). This investigates the type of degradation in the GERB instrument spectral response that could explain the observed changes.

Section 2 presents the data used in this study, whilst Section 3 details the methodology for the GERB-CERES matching. Section 4 presents the comparison results, including the theoretical investigation of instrument spectral response changes. A summary is provided in the final section.

2. Data

2.1. GERB data

The study uses GERB level-2 top-of-the-atmosphere (TOA) unfiltered SW radiances. It is noted that for unfiltered radiances here and throughout the paper, SW is used to refer to all reflected solar radiation. The native GERB observations are obtained at a spatial resolution of approximately 50 km at sub-satellite point and are affected by the non-uniform spatial weighting of the instrument Point Spread Function (PSF) and filtered by the instrument spectral response. The processing of all the GERB level 2 products uses finer spatial resolution narrowband data available from the Spinning Enhanced Visible and Infrared Radiometer Imager (SEVIRI, Schmetz et al., 2002) on the same satellite to geolocate the data, provide spectral and spatial detail needed to correct for imperfections in the GERB instrument spatial and spectral response, and provide information on the scene needed to enable a radiance to flux conversion. Several different GERB Level 2 products are available to users, all provided on a regular equal viewing angle grid at approximately 15 min temporal resolution but with slightly different spatial and temporal characteristics. The GERB product used here is the High-Resolution (HR) dataset (Dewitte et al., 2008), which has a resolution of 3 × 3 SEVIRI pixels (9 × 9 km at nadir) and is provided every 15 min as a snapshot of the radiances and fluxes at the time of SEVIRI data acquisition. Hence, within a given HR radiance field the observation time is matched to the SEVIRI scan pattern and thus varies with location. The HR product has 'enhanced' resolution with respect to the original GERB observations; this improved spatial resolution relies on normalised SEVIRI based broadband radiance estimates and overlap between the GERB pixel PSFs to provide information on the spatial variation of the scene within the GERB footprint. The SEVIRI narrowband to broadband relationships used for this are based on regressions performed on both a combination of simulated spectra and an observational dataset of matched broadband and SEVIRI measurements. It is noted that the GERB HR products are consistent with the native resolution GERB data at the larger GERB footprint scale and are designed to be used for creating custom averages. In fact, previous comparisons between GERB and CERES reported in Clerbaux et al. (2009) show that the HR product is actually best suited for comparisons with other instruments as it has the effect of the GERB PSF corrected and is not subject to temporal averaging. In addition to the unfiltered radiance, the angular information in the GERB HR product is also used for the observational matching performed here.

2.2. CERES data

For CERES, instantaneous TOA radiances are taken from Edition-3A of the Single Scanner Footprint (SSF) product (Wielicki et al., 1996). This study uses data from the FM1 instrument on the sun-synchronous Terra satellite (equator crossing times around 10:30 and 22:30 local time). FM1 is chosen as it is the instrument to which the other CERES instruments are calibrated for the Edition 3A products (Personal Comm, S. Thomas, December 2015). During the time period considered the FM1 instrument always operates in a cross-track scanning mode.

In addition to the unfiltered radiance, scene, angular information and measurements of the filtered radiance in the CERES SSF product are also used for matching and classifying data. The filtered radiance is the radiance that is directly measured by the instrument before spectral correction and includes the effect of the instrument spectral response. The unfiltered radiances, Rad_U, and filtered radiances, Rad_F are given by:

$$Rad_U = \int L(\lambda)d\lambda \quad (1)$$

$$Rad_F = \int L(\lambda)\varphi(\lambda)d\lambda \quad (2)$$

where λ is the wavelength, $L(\lambda)$ is the spectral radiance and $\varphi(\lambda)$ is the instrument spectral response. The unfiltered-to-filtered radiance ratio α is defined as:

$$\alpha = Rad_U / Rad_F \quad (3)$$

2.3. Simulated spectral radiance data

In Section 4, a study of the effects of a theoretical change in instrument spectral response is presented. For this purpose, a large database of simulated spectral radiance curves is used (Clerbaux et al., 2008; Clerbaux, 2008). The spectral radiance curves were simulated using the Santa Barbara DISORT Atmospheric Radiative Transfer (SBDART) model (Ricchiazzi et al., 1998), and are modelled for a wide variety of surface types for both clear and cloudy conditions. The surface types are formed as a combination of two fundamental geotypes such as ocean and vegetation (labelled 'primary' and 'secondary' with abundance), with the spectral reflectance curves of the geotypes themselves taken from the ASTER spectral library (Baldridge et al., 2009). Each scene type is simulated at a variety of different viewing geometries: solar zenith angles from 0° to 80° in 10° increments, viewing zenith angles from 0° to 85° in 5° increments and relative azimuth angles from 0° to 180° in 10° increments. 50% of the simulations include clouds, made up of high-, mid- and low-level overlapping layers. The altitude of the cloud layers is set at random with a uniform distribution of probability in the ranges 0.5–3.5 km (low), 4–7 km (mid) and 7.5–16 km (high). The respective optical thickness at 0.55 μm is also selected at random between 0.3 and 300 with a uniform distribution of probability. The low-level clouds are always composed of water droplets and the high-level clouds of ice crystals, with the phase of the mid-layer clouds either

water or ice with equal probability. The drop size distribution follows a gamma distribution stretched using the effective radius, which for water (ice) is uniformly selected at random from within the 2–25 μm (15–128 μm) range.

3. Methodology

The method of matching the observations for comparison largely follows that of previous work (e.g. Haeffelin et al., 2001; Clerbaux et al., 2009). The key objective is to achieve a sufficiently close spatial, temporal and angular match between the GERB and CERES radiance observations.

Spatial matching is achieved by modelling the CERES PSF as a disk with radius R_{PSF}, as described in Clerbaux et al. (2009), where the radius in km is given by:

$$R_{PSF} = 20/\cos(VZA_{CERES}). \quad (4)$$

Here VZA_{CERES} is the CERES viewing zenith angle. R_{PSF} is calculated for each CERES observation and the matched GERB radiance is calculated as a weighted average of all GERB HR pixels whose centres fall inside the CERES PSF disk. The weighting assigned to each contributing GERB HR pixel depends on the distance of its centre from the CERES PSF disk centre according to a Gaussian weighting function, with the Full Width Half Maximum (FWHM) taken to be R_{PSF}. Mathematically, the average GERB radiance $\overline{R_G}$ is given by:

$$\overline{R_G} = \sum_i e^{-\left(\frac{1}{2}\left(\frac{x}{\sigma}\right)^2\right)} R_{GHRi} \quad (5)$$

where x is the distance between the centre of GERB HR pixel i and the CERES PSF centre and

$$\sigma = R_{PSF}/\sqrt{2\ln 2} \quad (6)$$

The assumed shape of the CERES PSF is considered a reasonable simplification of the instrument response and has been shown by Clerbaux et al. (2008) to be sufficient to achieve a good match between GERB and CERES. The additional weighting used here brings the approximation closer to the characteristics of the actual CERES PSF (Priestley et al., 2010).

As noted in Section 2.1 the GERB HR product is provided at 15 min intervals, however the actual time associated with each observation will vary about this time depending on its location. Hence, for the temporal matching, a maximum absolute difference of 7.5 min is allowed between the times of the GERB and CERES observations.

For the angular matching a threshold value of 8° is chosen as the maximum allowed angle between the directions of the GERB and CERES observations. Sensitivity calculations from previous studies have shown that for angles smaller than this there is no significant improvement in comparison results (Clerbaux et al., 2009) and so 8° is used to maximize the number of matches between the two instruments.

To ensure the highest quality data are used several additional selection criteria are enforced in this study. Firstly, all GERB observations considered for comparison must have a viewing zenith angle and a solar zenith angle less than 60°. This is due to increased errors associated with higher viewing geometries (Russell, 2011). In order that all ocean scenes are identified correctly, a restriction is also made that the ocean sun-glint angle must be greater than 25°. Lastly, matches are only considered when both the GERB and CERES matched radiances are valid and non-zero (i.e. $>0\ W\ m^{-2}\ sr^{-1}$).

Fig. 1 shows the matched observations between GERB-1 and CERES FM1 for June 2008 given the restrictions detailed above. For all months of comparison in this study, the spatial range of matched observations is roughly similar (i.e. 50°W–50°E, 20°S–20°N). It is noted that although this spatial range of matched observations represents a limited percentage of the nominal GERB data range of 60°W–60°E, 60°S–60°N, the resulting measurements encompass a wide variety of different surface types ranging from ocean to desert to tropical rainforest biomes.

As previously discussed, we are attempting to diagnose and quantify the change in the GERB calibration over time. A previous intercomparison of GERB and CERES SW unfiltered radiances showed that the disparity between the measurements is best explained by multiplicative factors (Clerbaux et al., 2009). Studies carried out by the present authors (not shown) show that linear regressions between the GERB and CERES SW radiances produce intercepts that are extremely close to zero and

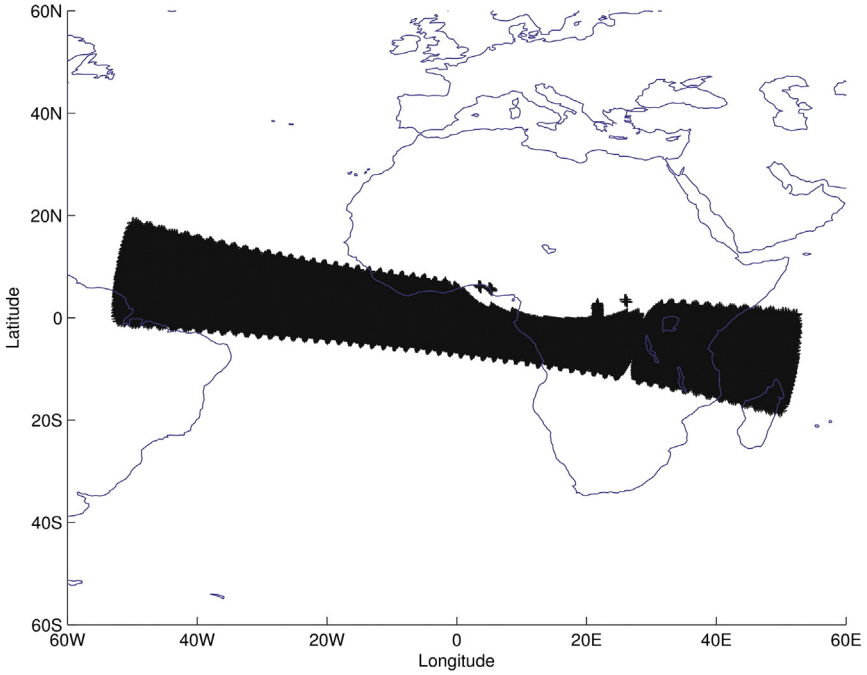

Fig. 1. Geographical location of the matched observations (in black) between the GERB-1 and CERES FM1 instruments for June 2008.

that this behaviour does not depend on the time period considered and does not contribute to the evolution in the difference between GERB and CERES SW radiance.

The expected aging mechanism of the optical components suggests that calibration changes will be dominated by a spectrally dependent loss of SW response. Such unaccounted for loss in instrument throughput would manifest as an error in the spectral correction of the broadband GERB measurements. This error will be a fraction of the observed radiance with the fractional value dependent on the spectral properties of the scene observed, thus at each point in time a wide range of fractional errors are expected in the dataset. To analyse the change we require a means to classify the data according to the magnitude of the fractional error experienced. Comparing without such a classification whether as a ratio or a regression will result in an apparently noisy picture with an average effect dependent on the precise makeup of scenes and their spectral distribution of energy. The classification must be sensitive enough to sufficiently limit the fractional change, but also able to group all scenes with the same spectral properties so to minimise comparison noise.

Following the example of Loeb et al. (2001), here we use the ratio of the unfiltered-to-filtered radiance to classify the spectral properties of different scenes, subsetting the data into narrow ranges of this ratio before comparison. Due to the effect of viewing and solar geometry for the range of observations considered this provides a much better characterisation of the spectral distribution of energy in the scene than could be obtained using the magnitude of the observed radiance, the bidirectional reflectance or a simple scene type classification such as overcast or clear ocean. Moreover, it can be shown to provide a much less noisy comparison for errors of this nature than can be obtained from comparisons classified by these other means (see Loeb et al., 2001). It also ensures that all scenes with the same spectral properties are included together, improving comparison signal to noise. This classification isolates within each subset a given fractional change which can be determined by considering the evolution in the ratio of GERB and CERES SW unfiltered radiances within that subset. Although a linear regression could in theory also be used after subsetting, some of the subsets have too narrow a range of radiances to make this approach robust, and given the negligible contribution of any offset the ratio is more appropriate for our purposes.

In this study for reasons of utility we use the CERES unfiltered-to-filtered radiance ratio rather than the equivalent quantity from GERB. Because of the similarity between the GERB and CERES optics (i.e. mirror coatings and filter material) this provides the appropriate sensitivity and separation although its absolute magnitude will differ from the corresponding GERB quantity due primarily to the different number of mirrors employed by the two instruments.

4. Results

4.1. Yearly comparisons

In the first instance, a comparison is made between CERES FM1 and GERB HR unfiltered radiances for every June and December between 2004 and 2006 (GERB-2) and 2007 and 2012 (GERB-1). Two "overlap" periods between GERB-2 and GERB-1 when both instruments were providing measurements, running from January 13th to February 11th 2007 and May 1st to May 10th 2007, are also considered. The numbers of CERES points matched (i.e. the number of matched observations) for all of these periods are shown in Tables 1–3.

Table 1
Number of matches between GERB-2 and CERES FM1 for June and December 2004–2006.

	2004	2005	2006
June	70,607	48,910	71,906
December	68,209	63,258	66,322

Table 2
As for Table 1, but for GERB-1 and CERES FM1 for June and December 2007–2012.

	2007	2008	2009	2010	2011	2012
June	75,751	76,464	77,303	76,149	76,294	71,507
December	36,277	39,033	68,516	66,074	55,867	65,866

Matches are classified into subsets according to the CERES unfiltered-to-filtered radiance ratio α_{FM1}. In general, the highest unfiltered-to-filtered radiance ratios correspond to the "bluest" scenes (e.g. clear dark ocean). For this analysis 46 subsets of the CERES FM1 unfiltered-to-filtered radiance ratios are used covering the range from $\alpha_{FM1} = 1.285$ to 1.400, with each interval having a width $\Delta\alpha_{FM1} = 0.0025$. The percentage of matched points in each unfiltered-to-filtered radiance ratio subset is shown in Fig. 2 for June 2004 (blue) and December 2008 (red). The shapes of these distributions are highly representative of what is seen across all the months and years considered in this study.

For each unfiltered to filtered radiance ratio subset a monthly comparison ratio M_α is calculated from the average of the matched GERB and CERES radiances:

$$M_\alpha = \frac{<Rad_{U,GERB,\alpha}>}{<Rad_{U,CERES,\alpha}>} \tag{7}$$

where $<Rad_{U,GERB,\alpha}>$ is the average of the matched GERB unfiltered radiances for that month in that subset of α with similar nomenclature applying for CERES. To obtain a measure of the variability through the month a daily comparison ratio $M_{\alpha,t}$ is calculated from the daily average of the matched unfiltered radiances in each α_{FM1} bin, viz.:

$$M_{\alpha,t} = \frac{<Rad_{U,GERB,\alpha,t}>}{<Rad_{U,CERES,\alpha,t}>} \tag{8}$$

for t = 1:N, where N is the number of days in the month. The variability is then calculated as three times the standard error in the sample

$$\varepsilon_\alpha = \frac{3\sigma(M_{\alpha,t})}{\sqrt{(N-1)}} \tag{9}$$

where σ is the standard deviation of the daily ratio. Following the example of Clerbaux et al. (2009) we use ε_α as a measure of the consistency within the month of the ratio calculated for each subset and show its size as bars around the overall monthly ratio in the following plots (Figs. 3, 4 and 5). To ensure a sufficient distribution of matched observations in the calculation of this variability, a daily $M_{\alpha,t}$ is only calculated if there are at least 50 matched observations in the relevant α_{FM1} and t bin.

4.1.1. GERB-2

Fig. 3 illustrates the monthly GERB/CERES SW unfiltered radiance ratios M_α, as a function of α_{FM1}, for GERB-2 for (a) June and (b) December 2004–2006. The associated variability through the month for each α, ε_α, is shown by the vertical error bars. For both June and December there is a broad decrease in M_α between 2004 and 2006 for all α_{FM1} bins. The average value of M_α calculated across all subsets of α_{FM1}, shows absolute decreases from 1.036 to 1.016 (June) and from 1.034 to 1.006 (December). These correspond to percentage decreases of 1.9% and

Table 3
As for Table 1, but considering both GERB-1 and GERB-2 versus CERES FM1 for two overlap periods, January 13th to February 11th 2007 and May 1st to May 10th 2007.

	13th Jan–11th Feb 2007	1st May–10th May 2007
GERB-2	59,573	22,526
GERB-1	63,029	76,687

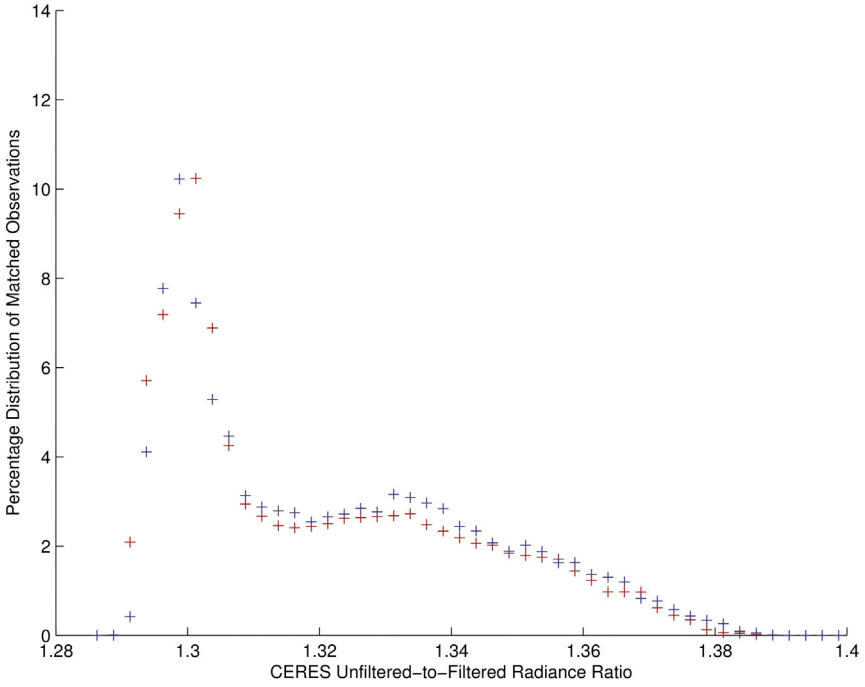

Fig. 2. Percentage of matched observations in each CERES unfiltered-to-filtered radiance ratio subset for GERB-2 and FM1 in June 2004 (red) and GERB-1 and FM1 in December 2008 (blue). (For interpretation of the references to colour in this figure legend, the reader is referred to the web version of this article.)

2.7% respectively. It is noted that the average GERB-2 radiances calculated across all subsets of α_{FM1} are 44.528 W m^{-2} sr^{-1} and 50.197 W m^{-2} sr^{-1} in June and December 2004, respectively.

However, the year-to-year changes are by no means consistent across all α_{FM1} subsets. Considering the June months, for values of $\alpha_{FM1} < 1.37$ a regular decrease is generally seen from year-to-year. However for $\alpha_{FM1} > 1.37$, this is not the case, with M_α noticeably larger in June 2006 than in June 2005. For the December months, a decrease is seen from year-to-year across all α_{FM1}, except in the range 1.3 to 1.32 where M_α appears to show little change between December 2005 and December 2006. Furthermore, for both the June and December months the largest percentage changes from year-to-year are noticeably larger for matched observations where α_{FM1} is >1.37. With reference to Fig. 2, this suggests that a minority of the overall matched observations

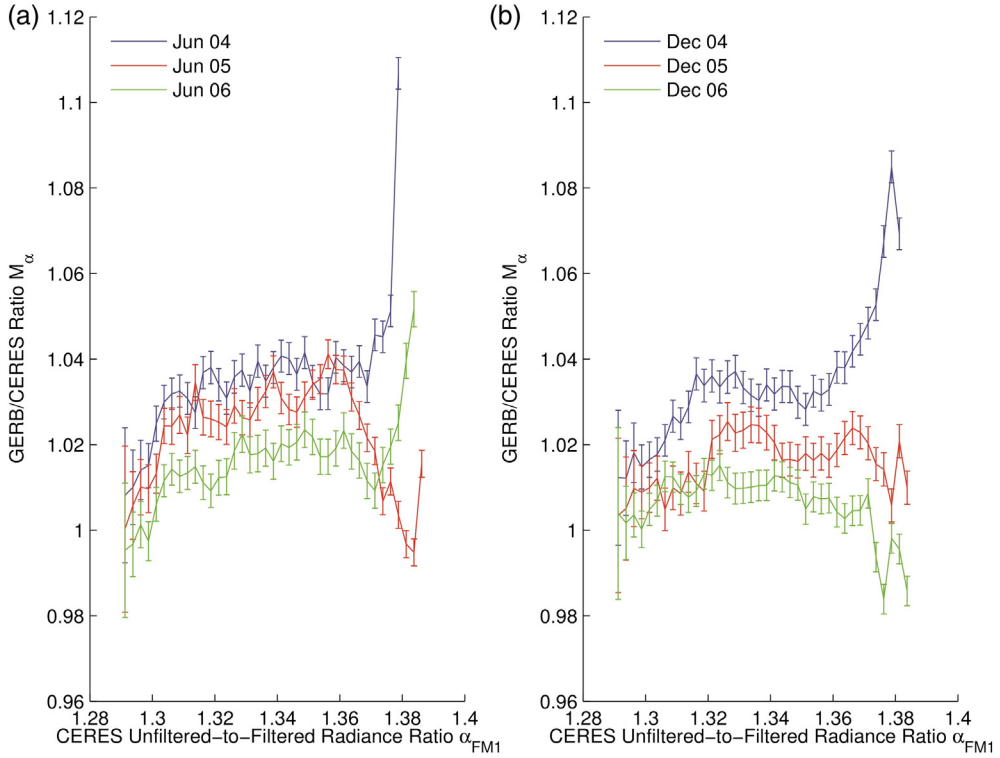

Fig. 3. GERB/CERES radiance ratios, M_α, as a function of CERES unfiltered-to-filtered radiance ratio subset, α_{FM1}, for (a) June 2004–2006 and (b) December 2004–2006. Each separate year is shown as a different colour in each individual figure. (For interpretation of the references to colour in this figure legend, the reader is referred to the web version of this article.)

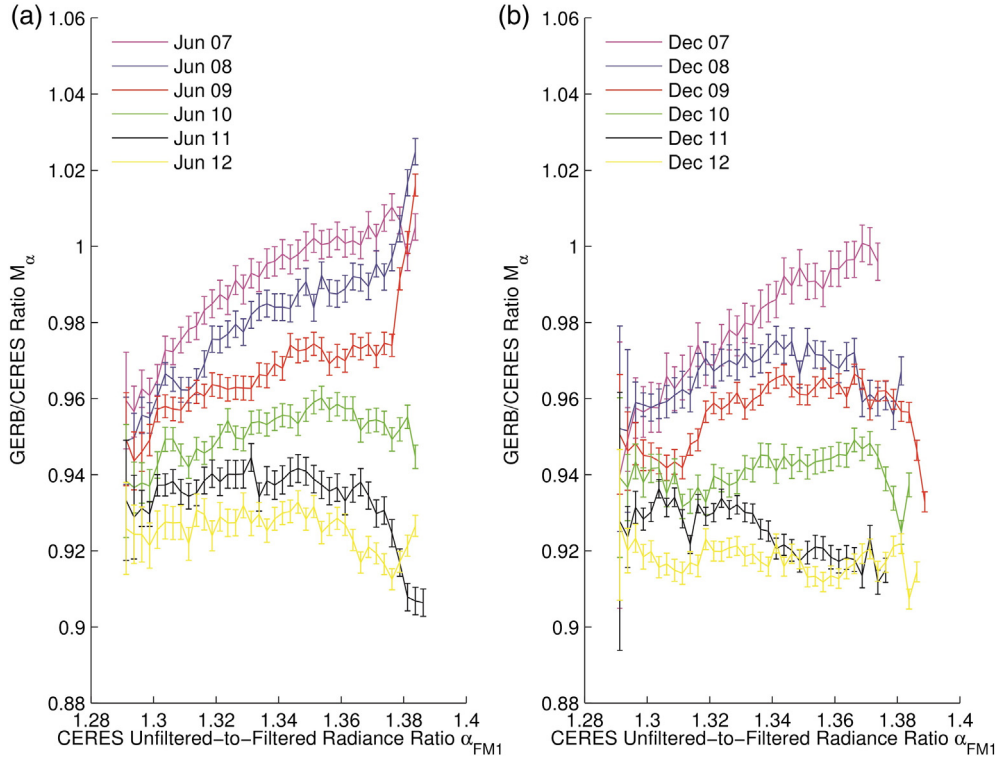

Fig. 4. GERB/CERES radiance ratios, M_α, as a function of CERES unfiltered-to-filtered radiance ratio subset, α_{FM1}, for (a) June 2007–2012 and (b) December 2007–2012. Each separate year is shown as a different colour in each panel. (For interpretation of the references to colour in this figure legend, the reader is referred to the web version of this article.)

are dominating the average values of M_α calculated using an equal weighting across the bins. As mentioned previously, these matched observations at the highest unfiltered-to-filtered radiance ratios correspond to the "bluest" scenes, which would be most sensitive to changes in the instrument SW spectral response at the shortest wavelengths in the visible and UV. We consider this further in Section 4.2.

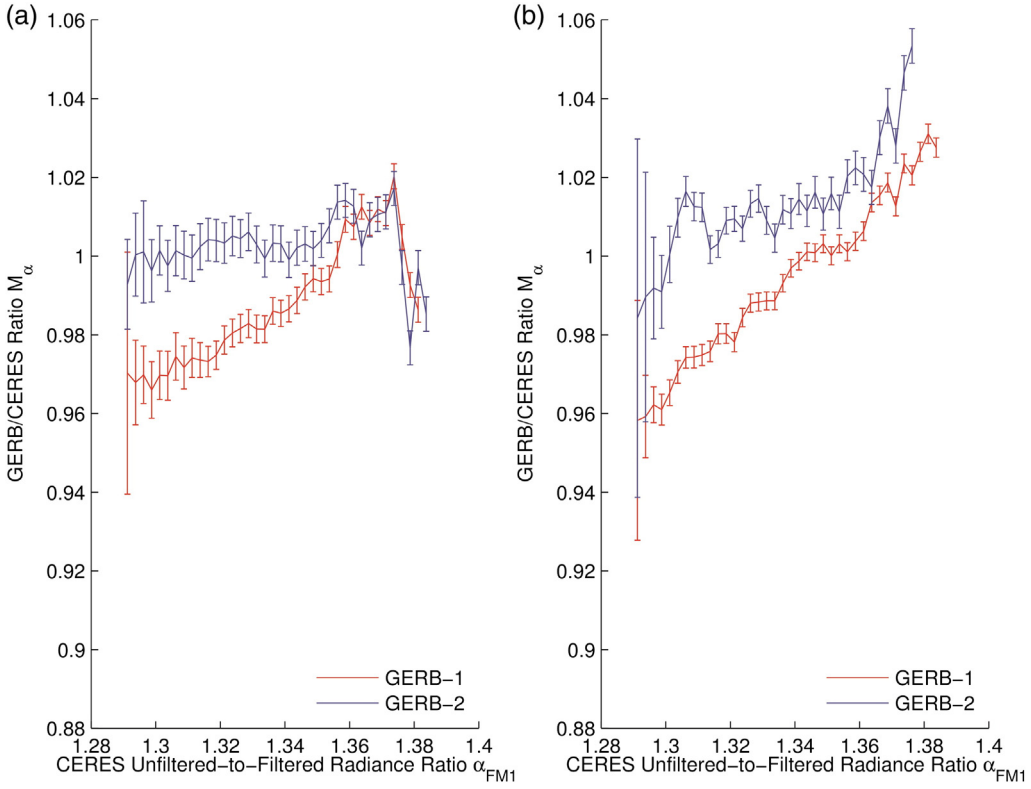

Fig. 5. GERB/CERES radiance ratios, M_α, as a function of CERES unfiltered-to-filtered radiance ratio subset, α_{FM1}, for (a) January 13th to February 11th 2007 and (b) May 1st to May 10th 2007.

4.1.2. GERB-1

Fig. 4 illustrates the GERB/CERES SW unfiltered radiance ratios M_α as a function of α_{FM1}, for GERB-1 for (a) June and (b) December for all years from 2007 to 2012. As for the previous comparisons, the associated variability estimates, ε_α, are shown by the vertical error bars. For both the June and December comparisons there is a marked decrease in M_α between 2007 and 2012. Between June 2007 and June 2012 (Fig. 4(a)), the average M_α, calculated across all values of α_{FM1}, decreases from 0.9899 to 0.9256, equating to a 6.5% decrease. At values of α_{FM1} <1.37, this decrease occurs at a consistent rate in each α_{FM1} bin but varies from bin to bin with the long-term decrease in M_α between June 2007 and June 2012 becoming larger as α_{FM1} increases. For α_{FM1} >1.37, whilst there is a clear long-term decreasing trend, M_α does not decrease consistently from year-to-year.

Between December 2007 and December 2012 (Fig. 4(b)), the average M_α calculated across all α_{FM1} decreases from 0.9782 to 0.9176, a 6.2% decrease. As for the June months, up to an unfiltered-to-filtered radiance ratio of 1.37, M_α is seen to decrease with time. However the rate of this decrease is not as consistent from year to year. This non-constant rate of change is even more apparent for α_{FM1} >1.37, although again there is a clear long-term decrease in M_α. In common with the June results, the long-term decrease in M_α between December 2007 and December 2012 becomes larger as α_{FM1} increases.

4.1.3. GERB-2/GERB-1 overlap periods

Fig. 5 shows M_α as a function of α_{FM1} for both GERB-2 and GERB-1 for (a) January 13th to February 11th 2007 and (b) May 1st to May 10th 2007. Again, the associated variability estimates, ε_α, are shown by the vertical error bars. Both overlap periods show that M_α is generally lower for GERB-1 than for GERB-2. For the first overlap period (Fig. 5(a)), averaging M_α across all α_{FM1} gives values of 1.0030 for GERB-2 and 0.9872 for GERB-1, corresponding to a 1.6% difference. This average offset is dominated by the larger differences at lower values of α_{FM1}; for α_{FM1} >1.37 there is a negligible difference. For the second overlap period (Fig. 5(b)), an average across all α_{FM1} gives values of 1.0131 for GERB-2 and 0.9934 for GERB-1, corresponding to a 1.9% difference. As for the first overlap period, this difference is dominated by the large changes at lower values of α_{FM1}, however there is now a noticeable difference between GERB-2 and GERB-1 at all α_{FM1}.

Between the first and second overlap periods, M_α shows an average increase of 1.0% for GERB-2 and 0.6% for GERB-1. This is mostly driven by changes in the higher unfiltered-to-filtered radiance ratios (α_{FM1} >1.37), which have been observed in all previous comparisons to be the unfiltered-to-filtered radiance ratios at which M_α is the most variable. It is noted that between the two overlap periods the two GERB instruments underwent orbital relocations in conjunction with the change of operations from Meteosat-8 (GERB-2) to Meteosat-9 (GERB-1), which could have contributed to the systematic offset between the two periods. Whilst such systematic effects will contribute an error to the determined absolute calibration difference between GERB and CERES, only data from a stable orbital position are used to study the evolution of the GERB 1 and 2 instrument calibrations. As such, they should be stable through the study period and should not affect the changes observed.

4.2. Attribution

For broadband observations such as those made by GERB and CERES, we may consider calibration errors due to changes in instrument response in terms of the discrepancy between the actual spectral response of the instrument (ϕ') and the spectral response assumed for the 'spectral correction' process (ϕ).

$$\Delta\phi(\lambda) = \phi\prime(\lambda) - \phi(\lambda) \tag{10}$$

Eqs. (1), (2) and (3) imply that the radiance actually measured by the instrument, Rad'_F, will be:

$$Rad\prime_F = \int L(\lambda)\phi'(\lambda)d\lambda \tag{11}$$

Spectrally correcting this measurement with the assumed spectral response, ϕ, will result in an error as the treatment will not correctly remove the effect of the true instrument spectral response ϕ'. This error will propagate to give an error in unfiltered-to-filtered radiance ratio, $\Delta\alpha$:

$$\Delta\alpha = \alpha' - \alpha = \frac{\int L(\lambda)d\lambda}{\int L(\lambda)\phi\prime(\lambda)d\lambda} - \frac{\int L(\lambda)d\lambda}{\int L(\lambda)\phi(\lambda)d\lambda} \tag{12}$$

Here α is the original unfiltered-to-filtered radiance ratio and α' is the unfiltered-to-filtered radiance ratio which should be applied to spectrally correct Rad'_F. The error in α will generate a corresponding error ΔRad_U in the derived unfiltered radiance Rad'_U:

$$Rad\prime_U = \alpha Rad\prime_F = \frac{\int L(\lambda)d\lambda}{\int L(\lambda)\phi(\lambda)d\lambda}\int L(\lambda)\phi'(\lambda)d\lambda = \frac{\alpha}{\alpha\prime}Rad_U \tag{13}$$

and

$$\Delta Rad_U = Rad\prime_U - Rad_U = \left(\frac{\alpha}{\alpha\prime} - 1\right)Rad_U \tag{14}$$

where Rad_U is the true unfiltered radiance as defined in Eq. (1).

The GERB/CERES radiance ratios, M_α, displayed as a function of unfiltered-to-filtered radiance ratio in Figs. 3–5, detail the disagreement between the GERB and CERES datasets due to differences in both calibration and processing. We anticipate the effects of processing differences to be stable through the record, as studies show (Russell, 2011) that the influence of the SEVIRI calibration and any change this is likely to experience has minimal impact on the GERB level 2 products. Indeed, these figures show that the differences clearly depend on, and evolve in time in a way that varies with, the unfiltered-to-filtered radiance ratio. In order to understand if the observed behaviour is consistent with what might be expected from theory, we first consider the effect of a SW darkening of the GERB spectral response which is most severe at the shortest wavelengths, such as that suggested by Matthews et al. (2005) where:

$$\phi\prime(\lambda)\begin{cases}\phi(\lambda)e^{a(\lambda-0.5)} & \lambda<0.5\mu m\\ \phi(\lambda) & \lambda\geq 0.5\mu m\end{cases} \tag{15}$$

with $a = -4\ln 0.4$. Applying this form of change to the GERB-2 spectral response results in the blue curve shown in Fig. 6, which has been superposed on the original GERB spectral response in red. Both curves were applied to the SBDART radiance database described in Section 2.3 to generate 750 values of α_G and α_G' (the G subscript indicating that they are derived from the GERB spectral response) encompassing a wide variety of scene types, solar illumination and observation angles. Fig. 7 shows the relationship between the fractional change in the unfiltered radiance $\Delta Rad_U/Rad_U$, given by (α_G/α_G') -1 (Eq. (14)), against the unfiltered-to-filtered radiance ratio α_G corresponding to the unaltered spectral response. The results clearly demonstrate how for this case the strong spectral signature of $\Delta\phi$ translates to an error in the unfiltered radiance which is linearly related to the magnitude of α_G. It is noted that the relatively small spread around the linear relation for all but the highest unfiltered-to-filtered radiance ratios (associated with the bluest ocean scenes) indicates that except in these extreme cases the spectral correction error is much less sensitive to the finer details of the scene, illumination and viewing geometry not captured in the unfiltered-to-filtered radiance ratio. Indeed, this highlights how the unfiltered-to-filtered radiance ratio is a good proxy for the spectral properties of the scene and can thus be useful for studying the effects

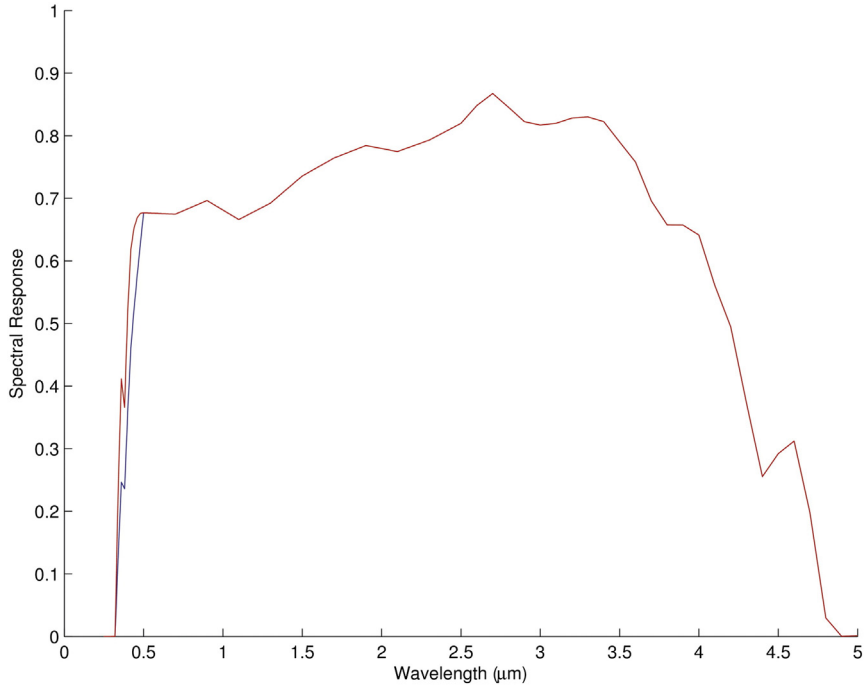

Fig. 6. GERB-2 start-of-life SW instrument spectral response (red). The simulated change in spectral response considered in this study, as described by Eq. (15), is shown in blue. (For interpretation of the references to colour in this figure legend, the reader is referred to the web version of this article.)

of instrument calibration differences. By contrast, a simple scene type classification such as 'cloud' or 'desert' does not isolate the change in the filtered radiance. Indeed, the results in Fig. 7 show that a wide range of fractional change is observed within these classifications.

As previously explained, for the purposes of this study we are not concerned with the start of life differences between the datasets: characterising the variation in their relative calibration with time is our primary goal. Fig. 7 shows how a fixed change to the GERB-2 spectral response that is not accounted for by a corresponding change in the GERB unfiltered-to-filtered radiance ratio will manifest as an error in the unfiltered radiance. This resulting error varies in a way that can be characterised by the unfiltered-to-filtered radiance ratio. Fig. 7 is an example of the error at a fixed point in time, so is analogous to the difference between the curves for different years shown for GERB 2 and GERB 1 in Figs. 3 and 4. When such an error increases with time, the increasing error in the unfiltered radiance will manifest in the radiance ratio M_α. Fig. 7 also indicates that any error in the unfiltered radiance, and hence M_α, shows little variation for a given unfiltered-to-filtered

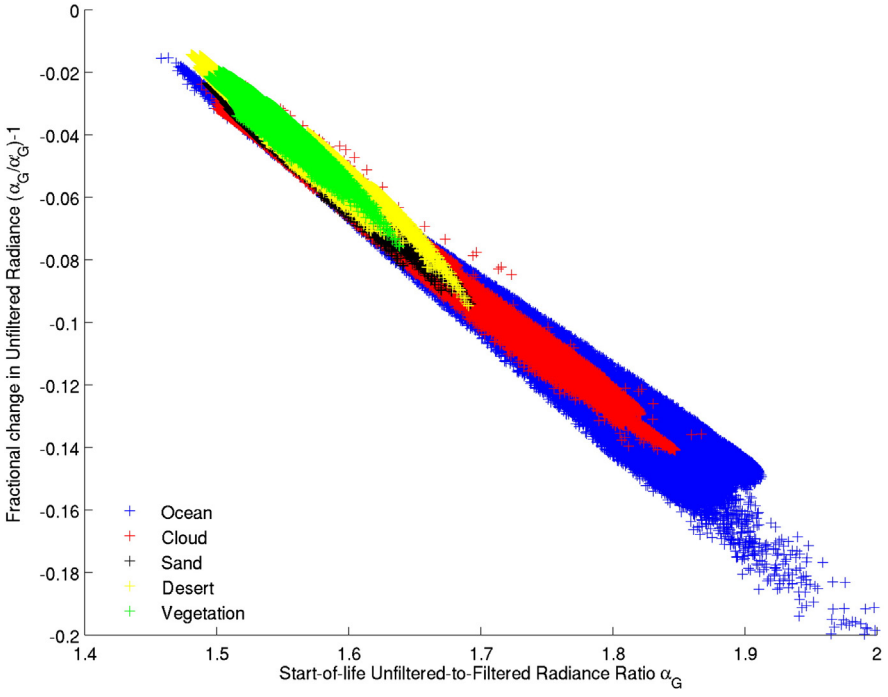

Fig. 7. The fractional change $\frac{\alpha_G}{\alpha'_G} - 1$ in the GERB-2 unfiltered-to-filtered radiance ratio resulting from the change to the GERB-2 SW spectral response shown in Fig. 6, as simulated by SBDART for a variety of different surface types.

Table 4
A list of months in which comparisons are made between GERB-2 and the CERES instrument FM1.

2004	2005	2006
Feb, May, June, Jul, Nov, Dec	Jan, May, Jun, Jul, Nov, Dec	May, Jun, Jul, Nov, Dec

radiance ratio, α_G. As such, given a stable CERES unfiltered radiance in the denominator of M_α, performing a time-series analysis of the evolution of M_α, stratified by unfiltered-to-filtered radiance ratio, should provide good insight into how both the magnitude and spectral characteristics of a change in instrument spectral response vary with time.

Assuming that errors in the CERES FM1 unfiltered radiance are stable over time, a statistical time-series analysis performed on M_α for both GERB-2 and GERB-1 can be used to study the calibration evolution of the GERB instruments. We note that for practical reasons the comparison uses α_{FM1} rather than α_G to stratify the radiance ratios. The similarity between the CERES and GERB instrument optics makes this substitution appropriate for our needs. As both employ the same UV enhanced silver coating on their mirrors and a quartz filter, for the SW channel the characteristic drop in response below 0.5 μm dominates the shape of the instrument spectral response and drives the scene variation of the unfiltered-to-filtered radiance ratio. As GERB uses five mirrors, compared to the two of CERES, the drop and hence range of unfiltered-to-filtered radiance ratios is larger for GERB, however studies (not shown) for the range of spectra covered by the SBDART radiance database demonstrate a simple linear relation between the unfiltered-to-filtered radiance ratios is expected for the two instruments. Thus, using the CERES unfiltered-to-filtered radiance ratios here should have no substantive effect on the calibration change derived, although an additional step will be needed to correctly map the change to the GERB scene. Tables 4 and 5 illustrate the comparison months included in this analysis. Values of M_α are calculated for each of these months and a linear regression fit on M_α with time is made separately for each α_{FM1} subset. The result of the linear regression provides an estimate of the monthly decrease in M_α, $\dot{M}_\alpha$, as well as a standard error on the estimate for each fit, SE_α. Fig. 8 illustrates two examples of these linear regression fits for GERB-2 for the subsets of α_{FM1} between 1.2975 and 1.3000 (black) and 1.3750 and 1.3775 (magenta). In these cases the linear fits produce values of $\dot{M}_\alpha$ and SE_α of 4.83×10^{-4} per month and 9.48×10^{-5} per month (black) respectively and 1.64×10^{-3} per month and 2.78×10^{-4} per month (magenta) respectively. Two further examples are shown in Fig. 9, for the same subsets of α_{FM1} but for GERB-1. In these cases, each linear fit produces values of $\dot{M}_\alpha$ and SE_α of 6.50×10^{-4} per month and 2.08×10^{-5} per month (black) respectively and 1.52×10^{-3} per month and 7.94×10^{-5} per month (magenta) respectively. Consistent with observations in Section 4, the change in M_α appears larger at the higher unfiltered-to-filtered radiance ratios (indicated by the higher values of $\dot{M}_\alpha$).

The differences between the GERB 1 and GERB 2 results are confirmed in Fig. 10, which plots $\dot{M}_\alpha$ and SE_α for every unfiltered-to-filtered radiance ratio subset for GERB-2 (red) and GERB-1(blue). For both GERB-2 and GERB-1, for all α_{FM1} $\dot{M}_\alpha$ is negative (i.e. M_α decreasing with time). In each case, the values of SE_α are substantially larger for unfiltered-to-filtered radiance ratios >1.37, indicating that at high α_{FM1}, the decrease in M_α with time is less clearly linear. Nevertheless, for α_{FM1} <1.37, SE_α for both instruments is reasonably small, suggesting that for all but the very bluest scenes the decrease in M_α is well fitted by a linear trend. It is noted that for the vast majority of points (α_{FM1} <1.37), the decrease in M_α is larger for GERB-1 then for GERB-2.

For both GERB-2 and GERB-1, the absolute magnitude of $\dot{M}_\alpha$ is seen to increase with α_{FM1}, indicating that M_α decreases faster at higher α_{FM1}. The variation of $\dot{M}_\alpha$ with α_{FM1} can be characterised by the slope, $\frac{d\dot{M}_\alpha}{d\alpha}$, determined from an error weighted linear regression fit. Each point is weighted in the regression with respect to the inverse of the square of its standard error (i.e. $\frac{1}{(SE_\alpha)^2}$,) such that more significance is given to the values of $\dot{M}_\alpha$ which are considered most accurate. For GERB-1, this weighted fit gives $\frac{d\dot{M}_\alpha}{d\alpha}$ as -0.0117 ± 0.0002 per month per unfiltered-to-filtered radiance ratio, where the error quoted is the standard error on the weighted fit. The ordinary R^2 for this fit is 0.99.

Eq. (14) showed that an error in the unfiltered radiance $(\frac{\alpha}{\alpha'}-1)Rad_U$, where Rad_U is the true unfiltered radiance, is introduced if filtered radiances are spectrally corrected with an assumed factor of α when in fact the true unfiltered-to-filtered radiance ratio is α′. Considering how this affects the GERB/CERES radiance ratio M_α over time, assuming that any error in the CERES FM1 unfiltered radiance is constant through time, from Eq. (14) we may write:

$$\dot{M}_\alpha = \left(\frac{\alpha_G}{\alpha'_G} - 1\right) \frac{Rad_{U,GERB}}{Rad_{U,CERES}} \tag{16}$$

where in this case $Rad_{U,GERB}$ and $Rad_{U,CERES}$ are the GERB and CERES unfiltered radiances at the start of the comparison period, α_G is the GERB unfiltered-to-filtered radiance ratio used to spectrally correct the GERB data (a constant for each instrument through the comparison period), and α'_G is the value of the unfiltered-to-filtered radiance ratio required at each time step to maintain a stable unfiltered GERB radiance equal to the start of comparison period value. It follows that:

$$\dot{M}_\alpha \propto \left(\frac{\alpha_G}{\alpha'_G} - 1\right) \tag{17}$$

Previously, it was shown that for the simulated SW darkening response given by Eq. (15), the factor $\frac{\alpha_G}{\alpha'_G}-1$ was linear with α_G. Given a linear relation between the GERB and CERES unfiltered-to-filtered radiance ratios, we may substitute $k\alpha_{FM1}$ for α_G (k is a constant), and thus retain the proportionality relation. As can be seen from Fig. 10, as well as from the standard error and the ordinary R^2 value of the weighted fit of $\dot{M}_\alpha$ versus α, for GERB-1 the variation of $\dot{M}_\alpha$ with α_{FM1} is highly linear. Assuming stable accuracy in the unfiltered radiances from FM1 over the comparison period, this result shows that the evolution of the GERB-1 unfiltered radiance calibration is consistent with the general type of SW darkening described by Eq. (15) and shown in Fig. 6, where the magnitude of SW darkening increases with decreasing wavelength.

For GERB-2 a weighted linear regression fit produces a value for $\frac{d\dot{M}_\alpha}{d\alpha}$ of -0.0082 ± 0.0009 per month per unfiltered-to-filtered radiance ratio, with an ordinary R^2 value of 0.71, suggesting the variation is less clearly linear than for GERB-1. Further attempts at non-linear regression with higher order polynomial and exponential fits produce poor fits. The results could be due to noise in the GERB-2 comparisons masking the linear decrease, a breakdown in the assumption of constancy for the CERES unfiltered radiance for this time period, or due to true non-

Table 5
As for Table 4, but for GERB-1.

2007	2008	2009	2010	2011	2012
Jun, Jul, Aug, Nov, Dec	Jan, Feb, May, Jun, Jul, Aug, Nov, Dec	Jan, Feb, May, Jun, Jul, Aug, Nov, Dec	Jan, Feb, May, Jun, Jul, Aug, Nov, Dec	Jan, Feb, May, Jun, Jul, Aug, Nov, Dec	Jan, Feb, May, Jun, Jul, Aug, Nov, Dec

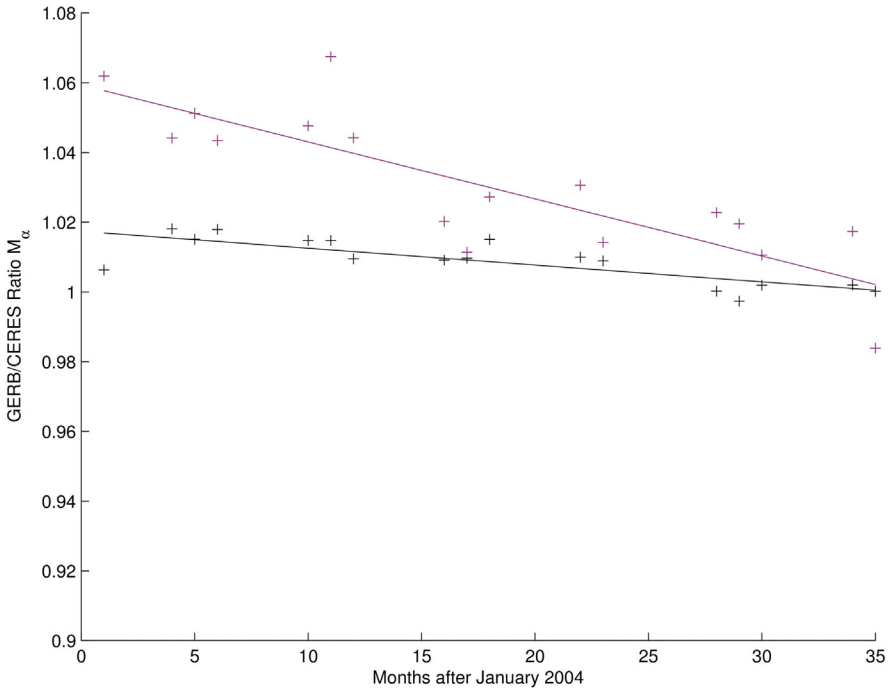

Fig. 8. Values of the GERB-2/CERES radiance ratios M_α calculated for each month in Table 4, for the subsets of α_{FM1} between 1.2975 and 1.3000 (black) and 1.3750 and 1.3775 (magenta). A linear regression is applied to each plot and the fitted line is plotted in their respective colour. (For interpretation of the references to colour in this figure legend, the reader is referred to the web version of this article.)

linear variations in the GERB-2 response evolution such as step changes driven by particular events. Such step changes would not be wholly unexpected for GERB-2 as it experienced two instrument anomalies during its operation which resulted in it directly viewing the sun and the loss of some GERB HR pixels. Although the GERB HR pixels lost are outside the comparison area these events would result in large instantaneous UV exposure to the primary optics which could potentially introduce step changes to the calibration. Nonetheless, the values of SE_α shown in Fig. 10 are still relatively small for GERB-2, indicating a reasonable degree of linearity in how M_α decreases with time at a particular unfiltered-to-filtered radiance ratio, implying there is a significant linear component to the GERB-2 evolution. Given that the values of $\dot{M}_\alpha$ for GERB-2 are of similar magnitude to those calculated for GERB-1 and are observed to decrease with α_{FM1}, this suggests that the linear component of the calibration evolution is a spectrally similar SW darkening loss of response.

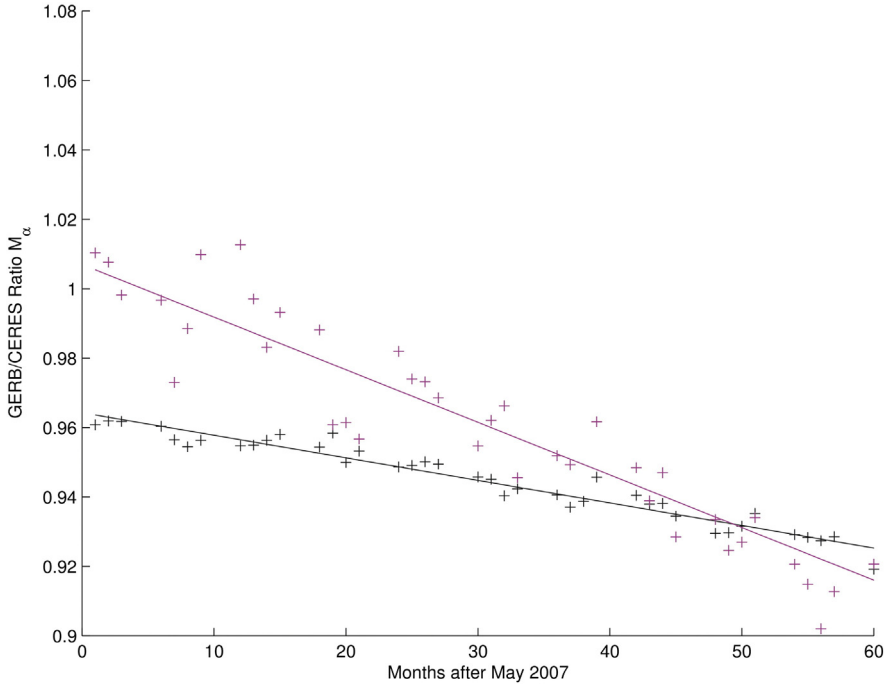

Fig. 9. As Fig. 8, but for GERB-1, for each month in Table 5.

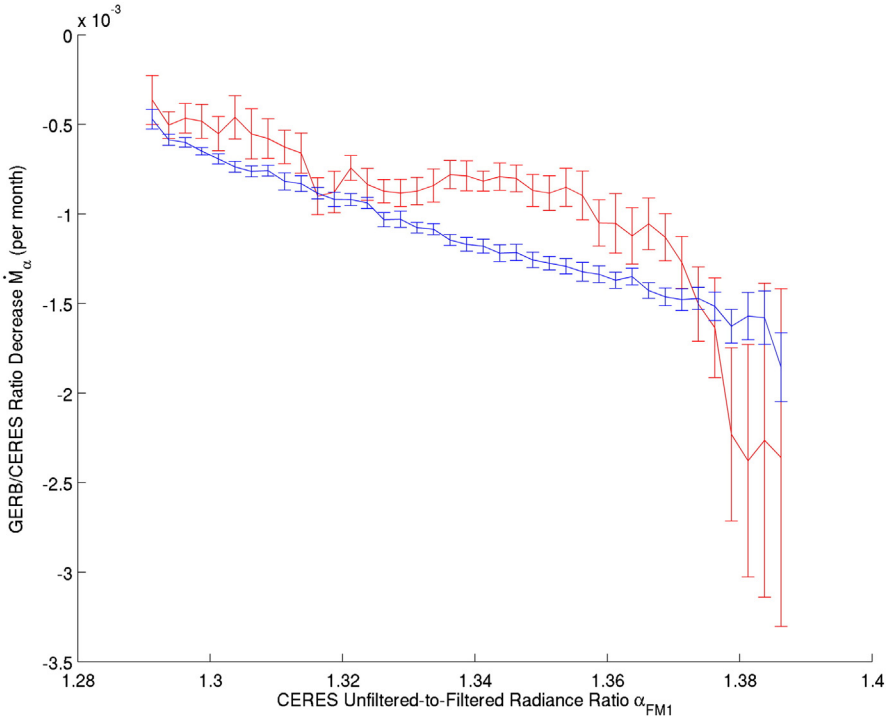

Fig. 10. The value of the monthly decrease in the ratio between GERB and the CERES FM1 unfiltered radiance, $\dot{M}_\alpha$, as fitted by linear regression for each subset in CERES unfiltered-to-filtered radiance ratio α_{FM1}, for GERB-2 (red) and GERB-1 (blue), for the months shown in Tables 4 and 5. Each value of $\dot{M}_\alpha$ is shown with the associated standard error, SE_α, of the fit. (For interpretation of the references to colour in this figure legend, the reader is referred to the web version of this article.)

5. Summary and discussion

In this study, the evolution of the GERB-2 and GERB-1 HR calibration has been investigated, through comparison with CERES Edition 3A SSF instantaneous radiances from FM1. These comparisons have been made by analyzing the evolution of monthly averaged GERB/CERES unfiltered radiance ratios, M_α, stratified as a function of CERES FM1 unfiltered-to-filtered radiance ratio, α_{FM1}. For GERB-2, between June (December) 2004 and June (December) 2006, M_α showed an average decrease of 1.9% (2.7%). For GERB-1, between June (December) 2007 and June (December) 2012, M_α showed an average decrease of 6.5% (6.2%). Two overlap periods, January 13th to February 11th 2007 and May 1st to May 10th 2007 were considered for both GERB-2 and GERB-1. On average, the GERB-1/CERES unfiltered radiance ratio was 1.6% (Jan–Feb) and 1.9% (May) smaller than the corresponding GERB-2/CERES unfiltered radiance ratio.

Further analysis showed that the evolution of M_α varied with the unfiltered-to-filtered radiance ratio of the scene. This implies that the magnitude of the decrease in M_α with time ($\dot{M}_\alpha$) is dependent on the spectral properties of the scene being observed. For GERB-1, further time-series analysis showed that $\dot{M}_\alpha$ was a linear function of the CERES unfiltered-to-filtered radiance ratio α_{FM1}, with the radiance ratios associated with the highest unfiltered-to-filtered radiance ratios (i.e. the bluest scenes) displaying the greatest monthly decrease. For GERB-2, the greatest monthly decrease was again found to occur at the highest unfiltered-to-filtered radiance ratios. However the regularity of the monthly decrease and the presence of a linear trend in its magnitude across the entire range of unfiltered-to-filtered radiance ratios were not as obvious as for GERB-1.

In order to better understand the nature of the calibration evolution, a theoretical study was performed considering the effect of spectrally varying shortwave darkening. Here, the GERB-2 start-of-life SW spectral response function was reduced according to the exponential function of wavelength derived by Matthews et al. (2005) as a fit to an observed change to the CERES spectral response. This altered GERB-2 spectral response function was then applied to simulated spectral radiance curves for a variety of different scenes and geometries to calculate associated unfiltered and filtered radiances. By comparison with the radiances calculated from the same curves, but with the original (unaltered) GERB-2 spectral response, the error which results if an appropriate update is not applied to the unfiltered-to-filtered radiance ratios was determined. The resulting error in the unfiltered radiance is given by the fractional change that should be made to the unfiltered-to-filtered radiance ratio and is a highly linear function of the original unfiltered-to-filtered radiance ratio. Assuming the accuracy of the CERES FM1 unfiltered radiance is constant over the comparison period, the evolution of the GERB unfiltered radiance error drives the observed decrease in the GERB/CERES unfiltered radiance ratio M_α. Thus it was shown that the rate of decrease of the ratio, $\dot{M}_\alpha$, is proportional to the fractional change required to correct the original unfiltered-to-filtered radiance ratio.

This study was concerned with the evolution of the GERB/CERES SW radiance ratio over time. The GERB SW fluxes are derived from the SW unfiltered radiance by application of a radiance to flux multiplier which depends on the scene and the solar and viewing geometry but not on the GERB radiance itself. Thus the multiplier itself is insensitive to the GERB calibration evolution and a given percentage change in the GERB SW radiance will manifest the same percentage change in the GERB SW flux. Under the assumption that CERES FM1 has stable calibration and that the unfiltered-to-filtered ratio isolates the magnitude of GERB calibration change, it can be shown that the fractional change in the GERB/CERES radiance ratio for a given unfiltered-to-filtered radiance ratio subset α_{FM1} will equal the fractional change in both the GERB SW unfiltered radiance and the GERB SW flux. For the most populated subset classification ($\alpha_{FM1} = 1.2975–1.3000$) the derived change to the GERB/CERES ratio M_α corresponds to an annual decrease of 0.8% in the ratio and hence in the GERB SW radiances and associated fluxes in this subset. For GERB-1 the annual decrease in the ratio for over 95% of the matched cases and hence expected in the GERB SW radiance

and associated flux is in the range 0.6% to 1.6%. For GERB-2 this corresponding range in annual decrease is 0.5% to 1.2%.

Is it reasonable to assume that CERES FM1 has a stable calibration? We consider that such an assumption is justified for the Ed 3A FM1 SW dataset used here as it is the result of extensive cross-validation checks that have been consistently performed on FM1 throughout time with the other CERES instruments, other instruments and various calibration targets (Loeb et al., 2006; Priestley et al., 2011; Shankar et al., 2014). These studies resulted in corrections being applied where needed in the Edition 3 processing to account for the type of spectral response changes studied in Matthews et al. (2005). Indeed, the remaining CERES flight models are inter-calibrated to FM1. With this assumption, the results reported here show that the GERB-1 Edition 1 unfiltered SW radiances have been systematically darkening over time due to a spectrally varying SW darkening of the GERB-1 spectral response function which is most pronounced at the shortest wavelengths.

Further work is required to refine the final correction that will need to be applied within the GERB calibration to account for this change and it is expected that additional studies including vicarious targets and extending the comparison to the full GERB field of the view will be made. However the results shown here clearly show that a correction to the GERB-1 unfiltered SW radiances or update to the GERB-1 unfiltered-to-filtered radiance ratios may potentially be applied as a linear trend in time and as a linear function of unfiltered-to-filtered radiance ratio. For GERB-2, although there is some similarity in the observed darkening, the variation in time is less well behaved and the variation of $\dot{M}_\alpha$ with unfiltered-to-filtered radiance ratio is not so obviously linear. This hints that changes to the GERB-2 SW spectral response may have occurred that are more variable in time and include more complex spectral components than those considered here. Nevertheless, much of the monthly decrease in M_α for each subset of α_{FM1} can be explained by a simple linear function, and a correction of this form should go much of the way to compensating for the GERB-2 calibration evolution.

Acknowledgments

This work was funded by EUMETSAT as part of the GERB 4 instrument programme. R. Bantges and H. Brindley are supported by NCEO grant PR140015. The authors are grateful to the Atmospheric Sciences Data Center at NASA Langley Research Center for providing the CERES data used in this work. The helpful comments of two anonymous reviewers are greatly acknowledged.

References

Baldridge, A.M., Hook, S.J., Grove, C.I., Rivera, G., 2009. The ASTER spectral library version 2.0. Remote Sens. Environ. 113, 711–715.
Clark, L.G., Dibattista, J.D., 1978. Space qualification of optical-instruments using NASA long duration exposure facility. Opt. Eng. 17 (5), 547–552.
Clerbaux, N., 2008. Processing of Geostationary Satellite Observations for Earth Radiation Budget Studies Doctoral Thesis.
Clerbaux, N., et al., 2008. Unfiltering of the Geostationary Earth Radiation Budget (GERB) data. Part I: shortwave radiation. J. Atmos. Ocean. Technol. 25 (7), 1087–1105.
Clerbaux, N., et al., 2009. Comparison of GERB instantaneous radiance and flux products with CERES Edition-2 data. Remote Sens. Environ. 113 (1), 102–114.
Dewitte, S., Gonzalez, L., Clerbaux, N., Ipe, A., Bertrand, C., De Paepe, B., 2008. The geostationary earth radiation budget edition 1 data processing algorithms. Adv. Space Res. 41 (11), 1906–1913.
Haeffelin, M., Wielicki, B., Duval, J.P., Priestley, K., Viollier, M., 2001. Inter-calibration of CERES and ScaRaB Earth radiation budget datasets using temporally and spatially collocated radiance measurements. Geophys. Res. Lett. 28, 167–170.
Harries, J., Russell, J., Hanafin, J., Brindley, H., Futyan, J., Rufus, J., et al., 2005. The geostationary earth radiation budget project. Bull. Am. Meteorol. Soc. 86 (7), 945–960.
Loeb, N., et al., 2001. Determination of unfiltered radiances from the clouds and the Earth's Radiant Energy System instrument. J. Appl. Meteo. V 40, 822–835.
Loeb, N., et al., 2006. Multi-instrument comparison of top-of-atmosphere reflected solar radiation. J. Clim. 20, 575–591.
Matthews, G., Priestley, K., Spence, P., Cooper, D., Walikainen, D., 2005, August. Compensation for spectral darkening of short wave optics occurring on the Cloud's and the Earth's Radiant Energy System. Optics & Photonics 2005 (pp. 588212–588212). International Society for Optics and Photonics.
Priestley, K.J., Thomas, S., Smith, G.L., 2010. Validation of point spread functions of CERES radiometers by the use of lunar observations. J. Atmos. Ocean. Technol. 27 (6), 1005–1011.
Priestley, K., et al., 2011. Radiometric Performance of the CERES Earth Radiation Budget Climate Record Sensors on the EOS *Aqua* and *Terra*Spacecraft through April 2007 Preistley et al. 2011 JAOT (V28 pp3–21).
Ricchiazzi, P., Yang, S., Gautier, C., Sowle, D., 1998. SBDART: a research and teaching software tool for plane-parallel radiative transfer in the Earth's atmosphere. Bull. Am. Meteorol. Soc. 79, 21012114.
Russell, J.E., 2011. Quality Summary for GERB EDITION 1. Available online at http://ggsps.rl.ac.uk/GERBED1_ARG_QS_v2.pdf.
Schmetz, J., Pili, P., Tjemkes, S., Just, D., Kerkmann, J., Rota, S., et al., 2002. An introduction to Meteosat Second Generation (MSG). Bull. Am. Meteorol. Soc. 83, 977–992.
Shankar, M., Priestley, K., Smith, N., Thomas, S., Walikainen, D., 2014. On-orbit stability and performance of the Clouds and Earth's Radiant Energy System (CERES) instrument sensors onboard the Aqua and Terra spacecraft. SPIE Optical Engineering + Applications (pp. 92180Q-92180Q). International Society for Optics and Photonics September.
Wielicki, B.A., Barkstrom, B.R., Harrison, E.F., Lee III, R.B., Smith, G.L., Cooper, J.E., 1996. Clouds and the Earth's Radiant Energy System (CERES): an earth observing system experiment. Bull. Am. Meteorol. Soc. 77, 853–868.